Estimation of three dimensional distributions of radiative properties by optical tomography

Nai-Rui Ou

Abstract

In this work, we develop and examine an optimization-based reconstruction scheme, which may estimate simultaneously the distribution of the extinction coefficient, the scattering albedo and the phase function of a three-dimensional inhomogeneneous medium. The forward radiative transfer problem with a complete scattering model is solved by a modified discrete-ordinate method. The inverse problem is formulated as a least square problem that minimizes the discrepancy between the measured and the calculated leaving radiative fluxes; the Levenberg-Marquardt algorithm is applied to the least square problems. From the results obtained, we found that the error caused by the estimated albedo does not result in the increase of error to the estimated extinction coefficient. For three-dimensional cases, when energy dissipation from both ends and property variation in z-direction for radiation intensity are not considerable, using the two-dimensional algorithm in place of the three-dimensional algorithm to reconstruct the radiative properties may generate accurate enough results and may save much computational time. The discrepancies between the estimated and exact values of the extinction coefficient and the scattering albedo increase with the increase of the measurement error, while the reconstructed coefficients of the expanded phase functions are less sensitive to the measurement error.

Keywords: three-dimensional inhomogeneneous media, extinction coefficient, scattering albedo, phase function, modified discrete-ordinate method.

Nai-Rui Ou, Associate professor, Department of Mechanical Engineering, HIT.
投稿日期：980514 接受刊登日期：980622

以光學斷層掃瞄法逆算三維分佈的熱輻射性質

歐乃瑞

摘 要

本文以求解精確的輻射傳遞的積微分方程式爲基礎，發展在完全的散射模式下，可同時逆算三維圓柱介質之吸收、散射性質及相函數的程式。我們以修正的離散方向法，求解柱狀介質受到側邊平行入射的正算問題，以所得的輻射熱通量爲模擬量測值，並用它與估算的輻射性質所求得的輻射熱通量之間的均方差，形成目標函數，然後再最小化此目標函數來逆算介質的性質。本文以 Levenberg-Marquardt 法來求解各個例子的最小均方問題。由結果得知，估算散射比所產生的誤差並不會導致增加估算消散係數產生的誤差。在三維的例子中，當能量從兩端散失不嚴重，且相關熱輻射性質 z 軸變化不顯著時，以二維的程式來逆算三維的例子，也可得到相當準確的結果，同時可以節省大量的運算時間。量測誤差的增加，會增加對散射比及消散係數的逆算結果的誤差的增加，然而，對相函數的逆算結果，顯得受量測誤差影響較少，也就是較不敏感。

關鍵詞：三維非均勻性介質、消散係數、散射比、相含數、修正離散方向法。

歐乃瑞：修平技術學院機械工程系副教授

I. INTRODUCTION

Optical tomography has wide applications in many areas[1-3, 6, 14, 16, 17] because it can provide estimates of the radiative properties of a scattering medium from boundary measurements of light leaving the medium. Among the light transport models employed by the optical tomography, the diffuse approximation is one of the most popular. The optical tomography based on the diffuse approximation is called diffuse optical tomography (DOT). The DOT is very successful in clinical applications [3,16], especially optically thick, strongly scattering cases. However, the DOT does not hold when the medium under consideration is not optically thick or includes low scattering regions.

To overcome the disadvantages of the DOT, several inverse schemes based on more rigorous light transport models have been developed. Yuen *et al*. [17] applied a generalized zonal method to estimate the extinction coefficient and the scattering albedo of a two-dimensional medium. Jiang [7] developed an inverse scheme based on higher-order diffusion approximations. Ripoll *et al*. [13] studied a radiosity-diffusion approach for media with non-scattering regions. Hill *et al*. [4] have presented a δ-Eddington variant of the diffuse approximation which could be improved to apply to the cases of both highly absorbing and highly scattering medium. Klose and Hielscher [8] reconstructed the scattering and absorption coeffiecients of a two-dimensional rectangular medium by solving the discrete-ordinate formulation of the transport forward model. Recently, Ou and Wu [11] developed an optimization-based reconstruction scheme, in which the foeward problem is solved by a modified discrete-ordinate method (MDOM) (Liou and Wu[9]). Their results show that the scheme can reconstruct accurate enough radiative properties of a scattering medium even for the cases with moderate optical sizes or low scattering. However, most of the cases they considered are two-dimensional.

In this work, we further examine the optimization-based reconstruction scheme for various three-dimensional cases with a complete scattering model. We also consider the application of a two-dimensional scheme reconstructing the radiative properties by using the measured data at a specific plane of the three-dimensional model. The two-dimensional scheme takes much less computer time than the three-dimensional scheme, and so the performance of the application of the two-dimensional scheme

to three-dimensional problem is worthy to examine.

II. ANALYSIS

To estimate the three-dimensional distributions of unknown radiative properties for a tubrid medium, we consider radiative transfer in an absorbing and scattering cylindrical cold medium with a transparent boundary exposed to a collimated beam, as shown in Fig. 1(a). The propagation direction of the radiation intensity at a point (r,ψ,z) can be specified by (ψ_x,θ), which are the angles between the propagation direction of radiation and a Cartesian coordinate, as shown in Fig. 1(b). Here, r, ψ and z denote the dimensionless coordinate r defined as the radial geometrical variable divided by the radius r_0, the azimuthal angle ψ and the dimensionless coordinate z defined as the axial geometrical variable divided by the radius r_0, respectively. The Boltzmann transport equation (BTE) of radiative transfer can be expressed as

$$\mu\frac{\partial}{\partial r}I(r,\psi,z,\psi_x,\xi)+\frac{\eta}{r}\frac{\partial}{\partial \psi}I(r,\psi,z,\psi_x,\xi)+\xi\frac{\partial}{\partial z}I(r,\psi,z,\psi_x,\xi)+\beta(r,\psi,z)\,I(r,\psi,z,\psi_x,\xi)$$
$$=\frac{\omega(r,\psi,z)\beta(r,\psi,z)}{4\pi}\times\int_{\psi'_x=0}^{2\pi}\int_{\xi'=-1}^{1}I(r,\psi,z,\psi'_x,\xi')\times\Phi(r,\psi,z,\psi_x,\xi,\psi'_x,\xi')d\xi'd\psi'_x$$
$$0\le r\le 1\ ,\quad 0\le\psi<2\pi\ ,\quad 0\le z\le z_0/r_0\quad 0\le\psi_x<2\pi\ ,\ -1\le\xi\le 1\ , \qquad (1)$$

where μ denotes the directional cosine defined as $\mu=\sin\theta\cos(\psi_x-\psi)$, I the radiation intensity nondimensionalized by the irradiation intensity I^i at $r=1$, $\psi=\psi^i$ and $z=z^i$ along the direction defined by $\mu=-1$ and $\xi=0$, η the directional cosine defined as $\eta=\sin\theta\sin(\psi_x-\psi)$, ξ the directional cosine defined as $\xi=\cos\theta$, β the dimensionless extinction coefficient defined as $(\kappa+\sigma_s)r_o$, with k and σ_s denoting the absorption and scattering coefficient, respectively, ω the scattering albedo defined as $\sigma_s/(\kappa+\sigma_s)$, and Φ the scattering phase function expressed in the form

$$\Phi(r,\psi,z,\psi_x,\xi,\psi'_x,\xi')=\sum_{k=0}^{K}A_k(r,\psi,z)P_k(\cos\theta_o)\ . \qquad (2)$$

Here, K denotes the order of anisotropic scattering, A_k the coefficient of the expansion with $A_0=1$, P_k the kth-order Legendre polynominal, and $\theta_o=\cos^{-1}(\mu\mu'+\eta\eta'+\xi\xi')$. The three

parameters, β, ω and Φ, may vary radically, azimuthally and axially. Here, we assume that the particles are spherical, and so the phase function is described by the angle formed by the direction of incident ray and the forward direction of the scattered ray (θ_o) only. The boundary condition for this problem can be expressed as

$$I(1,\psi,z,\psi_x,\xi) = \begin{cases} 1 & \text{at } \psi=\psi^i,\ z=z^i,\ \mu=-1,\ \xi=0, \\ 0 & \text{otherwise,} \end{cases}$$

$$0\le\psi<2\pi \quad , \quad -1\le\xi\le 1 \quad , \quad 0\le z\le z_0/r_0 \quad ,$$

$$\pi/2\le(\psi_x-\psi)\le 3\pi/2 . \tag{3}$$

Eqs. (1) and (3) form the forward problem.

Before solving the forward problem, we decompose the intensity into the fairly diffuse part I^d and the collimated part I^c (Liou and Wu, 1997; Hsu *et al*., 1998). The latter is zero except that

$$I^c(r,\psi,z,\psi^i+\pi,0)=e^{-\tau_c(r,\psi,z)}$$

$$\text{for } \psi=\psi^i \text{ or } \psi=\psi^i+\pi,\ z=z^i \tag{4}$$

with

$$\tau_c(r,\psi,z) = \begin{cases} \int_r^1 \beta(r',\psi^i,z)dr' \\ \quad \text{for } \psi=\psi^i,\ z=z^i \\ \int_0^1 \beta(r',\psi^i,z)dr'+\int_0^r \beta(r',\psi^i+\pi,z)dr' \\ \quad \text{for } \psi=\psi^i+\pi,\ z=z^i \end{cases} \tag{5}$$

By substituting Eqs. (4) and (5) into Eq. (1), we obtain the transport equation for I^d,

$$\begin{aligned} &\mu\frac{\partial}{\partial r}I^d(r,\psi,z,\psi_x,\xi) \\ &+\frac{\eta}{r}\frac{\partial}{\partial\psi}I^d(r,\psi,z,\psi_x,\xi) \\ &+\xi\frac{\partial}{\partial z}I^d(r,\psi,z,\psi_x,\xi) \\ &+\beta(r,\psi,z)\,I^d(r,\psi,z,\psi_x,\xi) \\ &=\frac{\omega(r,\psi,z)\beta(r,\psi,z)}{4\pi} \\ &\quad\times\int_{-1}^{1}\int_0^{2\pi} I^d(r,\psi,z,\psi_x',\xi') \\ &\quad\times\Phi(r,\psi,z,\psi_x,\xi,\psi_x',\xi')d\psi_x'd\xi' \\ &+\frac{\omega(r,\psi,z)\beta(r,\psi,z)}{4\pi} \\ &\times\Phi(r,\psi,z,\psi_x,\xi,\psi^i+\pi,0)\ , \\ &\times I^c(r,\psi,z,\psi^i+\pi,0) \\ &0\le r\le 1 \quad , \quad 0\le\psi<2\pi \quad , \quad 0\le z\le z_0/r_0 \quad , \\ &0\le\psi_x<2\pi\ , \ -1\le\xi\le 1 \end{aligned} \tag{6}$$

The boundary condition for I^d is

$$\begin{aligned} &I^d(1,\psi,z,\psi_x,\xi)=0 \\ &0\le\psi<2\pi \quad , \ 0\le z\le z_0/r_0 \quad , \quad -1\le\xi\le 1 \quad , \\ &\pi/2\le(\psi_x-\psi)\le 3\pi/2 , \\ &I^d(r,\psi,z_0/r_0,\psi_x,\xi)=0 \\ &0\le r\le 1, 0\le\psi<2\pi\ , \ -1\le\xi\le 0 , \\ &I^d(r,\psi,0,\psi_x,\xi)=0 \qquad\qquad 0\le r\le 1 \quad , \\ &0\le\psi<2\pi\ , \ 0\le\xi\le 1 . \end{aligned} \tag{7}$$

We adopt a DOM scheme (Hsu *et al*., 1998) to solve $I^d(r,\psi,z,\psi_x,\xi)$. The

discrete-ordinate approximation of Eq. (6) can be expressed as:

$$\mu_{n,m}(\psi)\frac{\partial}{\partial r}I^d_{n,m}(r,\psi,z)$$
$$+\frac{\eta_{n,m}(\psi)}{r}\frac{\partial}{\partial \psi}I^d_{n,m}(r,\psi,z)$$
$$+\xi_m\frac{\partial}{\partial z}I^d_{n,m}(r,\psi,z)$$
$$+\beta(r,\psi,z)I^d_{n,m}(r,\psi,z)=\frac{\omega(r,\psi,z)\beta(r,\psi,z)}{4\pi}$$
$$\times\left\{\left[\sum_{n'=1}^{N_{\psi_x}}\sum_{m'=1}^{M_\theta}I^d_{n',m'}(r,\psi,z)\right.\right.$$
$$\left.\times\Phi_{n,,m,n',m'}(r,\psi,z)w_{n',m'}\right]$$
$$\left.+\Phi_{n,m,n^i,m^i}(r,\psi,z)I^c{}_{n^i,m^i}(r,\psi,z)\right\}$$

for $0\le r\le 1$, $0\le\psi<2\pi$, $0\le z\le z_0/r_0$, n=1, 2, …, N_{ψ_x}, m=1,2, …, M_θ,

(8)

where the subscripts n and m represent the discrete directions, $w_{n',m'}$ the quadrate weight, the subscripts n^i, m^i the direction of incident radiation, N_{ψ_x} and M_θ the numbers of discrete ordinates over $0\le\psi_x\le 2\pi$ and $-\pi/2\le\theta\le\pi/2$, respectively. We divide the whole domain into $N_r\times N_\psi\times N_z$ cells, where N_r, N_ψ and N_z denote the numbers of cells in the r, ψ and z directions, respectively. The finite-difference approximation of Eq. (8) is solved by Gauss-Seidel method. Solving the BTE by splitting the radiative intensity into the exact I^c and the discrete-ordinates approximation of I^d is called the modified DOM (Liou and Wu, 1997).

To illustrate the reconstruction process, we consider radiative transfer in a medium composed of two species with variable concentrations. One of the species is non-scattering but absorptive, the other is both scattering and absorptive. For example, the mixture of Intralipid solution and India ink. The radiative properties of such a medium can be described by a variable extinction coefficient, a variable scattering albedo and a constant phase function. The unknown distributions of the extinction coefficient, the albedo and the phase function are expressed as

$$\hat{\beta}(r,\psi,z)=a_{000}$$
$$+\sum_{m=1}^{\hat{M}_\beta}\sum_{n=0}^{\hat{N}_\beta}\sum_{l=1}^{\hat{L}_\beta}r^m\left[a_{mnl}\cos(n\psi)+b_{mnl}\sin(n\psi)\right]z^l$$
$$+\sum_{m=1}^{\hat{M}_\beta}a_{m00}r^m+\sum_{l=1}^{\hat{L}_\beta}a_{00l}z^l$$
$$0\le r\le 1,\ 0\le z\le z_0/r_0,0\le\psi<2\pi,\quad(9)$$
$$\hat{\omega}(r,\psi,z)=c_{000}$$
$$+\sum_{m=1}^{\hat{M}_\omega}\sum_{n=0}^{\hat{N}_\omega}\sum_{l=1}^{\hat{L}_\omega}r^m\left[c_{mnl}\cos(n\psi)+d_{mnl}\sin(n\psi)\right]z^l$$
$$+\sum_{m=1}^{\hat{M}\omega}c_{m00}r^m+\sum_{l=1}^{\hat{L}_\omega}c_{00l}z^l$$
$$0\le r\le 1,\ 0\le z\le z_0/r_0,0\le\psi<2\pi,\qquad(10)$$

and

$$\hat{\Phi} = \sum_{k=0}^{\hat{K}} \hat{A}_k P_k(\cos\theta_o)$$

$0 \le r \le 1$, $0 \le z \le z_0/r_0$, $0 \le \psi < 2\pi$, respectively. (11)

Now, to reconstruct the radiative properties of the medium is equivalent to find the coefficients, $\hat{A}_k$, a_{000} , a_{mnl} , b_{mnl} , c_{000} , c_{mnl} and d_{mnl} . Here, we try to find those coefficients by minimizing the objective function

$$F = \sum_{i=1}^{N_i}\sum_{j=1}^{N_\psi}\sum_{k=1}^{N_z}\left\{ \tilde{q}^i_{N_r+1/2,j,k} - \hat{q}^i_{N_r+1/2,j,k}\left[\hat{\beta},\hat{\omega},\hat{\Phi}\right] \right\}^2 ,$$

$j \ne j^i$ and $k \ne k^i$, (12)

where *i* denotes the *i*-th incidence, N_i the total number of incidences, $\tilde{q}^i_{N_r+1/2,j,k}$ and $\hat{q}^i_{N_r+1/2,j,k}$ the measured and estimated leaving radiative fluxes in the radial direction at the boundary $(1,\psi,z)$, respectively. To gain enough information for reconstructing the three dimensional distribution of radiative properties, we scan the incident laser beam around the peripheral of medium at N_ψ locations on the same $r-\psi$ plane and then proceed along the z direction. At every $r-\psi$ plane we scanned, the incident locations are equally spaced by the azimuthal angle $\Delta\psi = 2\pi/N_\psi$. While the incident radiation enters the domain at a different location, we measure the other set of the leaving radiative fluxes. $N_\psi \times N_z - 1$ measured data are acquired for every incidence, which is equal to because the incident point is excluded. By N_i times of incidences and $N_\psi \times N_z - 1$ measured data generated for every incidence, $N_i \times (N_\psi \times N_z - 1)$ measured data can be obtained to reconstruct the radiative properties. To determine those unknowns, the number of the measured data $N_i \times (N_\psi \times N_z - 1)$ shall be greater than the number of unknowns,

$$2\times[\hat{M}_\beta \times (\hat{N}_\beta + 1)\times \hat{L}_\beta] + \hat{M}_\beta + \hat{L}_\beta$$
$$+ 2\times[\hat{M}_\omega \times (\hat{N}_\omega + 1)\times \hat{L}_\omega] + \hat{M}_\omega + \hat{L}_\omega + \hat{K} + 3$$

The leaving radiative flux caused by the *i*-th incidence could be expressed as:

$$q^i_{N_r+1/2,j,k} = \begin{cases} \sum_{n=1}^{N_{\psi x}}\sum_{m=1}^{M_\theta} I_{N_r+1/2,j,k,n,m}\mu_{j,n,m}w_{n,m} + I^c{}_{N_r+1/2,j^i,k^i,n^i,m^i}, \\ j = j^i + N_\psi/2 \quad \text{and} \quad z = z^i \\ \sum_{n=1}^{N_{\psi x}}\sum_{m=1}^{M_\theta} I_{N_r+1/2,j,k,n,m}\mu_{j,n,m}w_{n,m}, \\ j \ne j^i + N_\psi/2 \ \text{ or } \ z \ne z^i \end{cases}$$

for $\mu_{j,n,m} > 0$. (13)

The steps of reconstructing radiative properties are summarized as follows:

1. Guess the properties $\hat{\beta}$, $\hat{\omega}$ and $\hat{\Phi}$ by setting parameters $a_{mnl} = 0$, $b_{mnl} = 0$, $c_{mnl} = 0$, $d_{mnl} = 0$ and $\hat{A}_k = 0$, except

that $a_{000}=1$, $c_{000}=0.1$ and $\hat{A}_0=1$.

2. Solve the forward problem and obtain $\hat{q}^i_{N_r+1/2,j,k}(\hat{\beta},\hat{\omega},\hat{\Phi})$ by the DOM.
3. Find the new estimation of parameters a_{mnl}, b_{mnl}, c_{mnl}, d_{mnl} and $\hat{A}_k$ by minimizing the objective function. A standard least-square optimization procedure, the Levenberg-Marquardt algorithm (Marquardt, 1963; William *et al*., 1992) is used here.
4. Stop the iteration, if the two successive estimated values of a_{mnl}, b_{mnl}, c_{mnl}, d_{mnl} and $\hat{A}_k$ meet one of the following specified criterions. Otherwise return to step 2 with the newest set of estimated parameters.

The stopping criterions are as follows: (i) on two successive iterations each of the parameters agrees to 6 digits, (ii) on two successive iterations the relative difference of the objective functions is less than 10^{-8}, (iii) the Euclidean norm of the approximate gradient of the objective function is less than 10^{-8}.

III. RESULTS AND DISCUSSION

The inverse scheme is based on an iterative, optimization-based reconstruction method that minimizes the discrepancy between measured and calculated radiative fluxes. To ensure the accuracy of the calculated radiative fluxes, we first examine the effects of the numbers of the cells and the discrete ordinates on the solutions of the forward problem. The extinction coefficient (β_3) and the phase function (Φ_f) are listed in Table 1. The forward scheme is applied to a typical example with $\beta=\beta_3$, $\Phi=\Phi_f$, $\omega=0.5$, $z_i=0.5$, $A=1$ and $H=1$. Figs. 2(a) and 2(b) show that the distributions of the diffuse part of the radiative heat flux (q^d) around the peripheral boundary on the $r-\psi$ plane and along the line ($r=1,\psi=\pi/2$), respectively. The comparisons show that the results for $40\times96\times40$ and $20\times48\times20$ cells are in good agreement. Next, we consider the other example with the peak-like distribution of the extinction coefficient β_2, listed in Table 1. From Figs. 3(a) and 3(b), the deviation is larger for fewer numbers of cell, especially for those distributions near the path of incident light. The distribution near the incident path may cause larger error because of the non-uniform character of the collimated incidence and the fewer times of scattering. Hence, more cells are necessary when the distribution of the extinction coefficient becomes more non-uniform.

Figs. 4 shows the diffuse heat flux distributions along z-axis direction at $r=1$ and $\psi=\pi/2$ with the same relevant parameters as in Fig. 2(a). The domain is divided into $N_r \times N_\psi \times N_z = 20 \times 48 \times 20$ cells. Evidently, we can get the convergent result by increasing the numbers of discrete directions. The deviation near the incident path for the case of $M \times N = 4 \times 1$ show that fewer times of scattering may lead to larger errors and more discrete ordinates is necessary.

Figs. 5(a) and 5(b) show the distribution of the diffuse radiative flux ratio along the axes at $r=1,\ \psi=\pi/2$ and $r=1,\ \psi=\pi$ for three different values of albedo. The domain is divided into $N_r \times N_\psi \times N_z = 10 \times 24 \times 10$ cells and $N_{\psi_x} \times M_\theta = 12 \times 5$ discrete ordinates are adopted. The extinction coefficient β_1 listed in Table 1 is considered with $\Phi = \Phi_f$, $z_i = 0.5$, $A=1$ and $H=1$. The results show the ratios of the diffuse radiative flux distributed along the axis become larger for larger albedo. This is because that larger albedo means more scattering within the medium. Hence, the energy could be transferred easily along the axial direction that perpendicular to the incident direction.

Fig. 6 shows the distribution of the diffuse radiative fluxes for different optical thickness along the axes that are parallel to *z*-axis passed through the points $r=1,\ \psi=\pi/2$, $r=1,\ \psi=\pi$ and $r=1,\ \psi=3\pi/2$, respectively. At the axis $r=1,\ \psi=3\pi/2$, the curve has a higher peak for optical by thin case and then drop dramatically under the curve of the optical by thick case. Less incident radiation absorbed for the optical by thin case and the forward scattering aligned with the direction of incidence both enforce the higher peak. Away from the incident path, the scattered light easily leaves the optical by thin medium, so the radiative distributions are higher for the optical by thick case. The leaving radiative fluxes do not align with the incident direction at the other two axes. Thus, the peak and the distributions are higher than those of the optical thick case. The results show more light scattered flux transfer axially for the optically thick case.

Now, we turn to the inverse problems. In the reconstruction process, we rotate the incident beam around the peripheral of every incident plane and then move along z-axis direction axially. By doing this, at every incident we collect the measured q^d leaving lateral boundary at all grids except those at the incident point and the edge grids with $z=0$ and $z=z_0/r_0$. The

calculated q^d are obtained by solving the radiative transfer equation along $N_{\psi_x} \times M_\theta = 12 \times 5$ discrete ordinates and divide the domain into $N_r \times N_\psi \times N_z = 10 \times 24 \times 10$ cells. The comparisons in Figs. 2-4 have shown that for the direct problems the numbers of cells and discrete ordinates are enough for smooth radiation parameters. The effects of the numbers of cells and discrete ordinates will be further examined for the inverse problem. The aspect ratio (A) and the dimensionless height (H) are all unity in the following cases. For the three dimensional inverse problem, the incident planes are z =0.5, 0.75 and 0.95, respectively. Hence, N_i is equal to $N_\psi \times 3$ and N_I equal to $N_\psi \times N_z - 1$.

To estimate the three-dimensional distribution of the extinction coefficient, we first consider the case with $\beta = \beta_3$, $\omega = \omega_1$ and $\Phi = \Phi_f$. The exact (β) and estimated distributions of the extinction coefficient ($\hat{\beta}$) along the *x*-, *y*- axis at plane $z = 0.5$ and line $(0.2, 0, \mathrm{z})$ are shown in Figs. 7(a), (b) and (c), respectively, where the $\hat{\beta}$ is obtained by the expansion with $\hat{M}_\beta \times \hat{N}_\beta \times \hat{L}_\beta = 5 \times 3 \times 3$. In Fig. 7(a), it shows a little deviation for $x > 0.5$. The reason may be that the distribution of β makes the optical size larger for $x > 0.5$. In Fig. 7(b), the deviation appears near incident path because non-uniform character of the collimated incidence and the fewer times of scattering. In Fig. 7(c), results around both ends (top and bottom) show less accurate. The reasons may be attributed to (i) energy dissipation from both ends and (ii) abrupt variation due to finite length in z-direction for radiation intensity near both ends. Increasing the numbers of cells in ψ-direction up to 48 could improve the accuracy obviously as shown in Figs. 7(a), 7(b) and 7(c), respectively.

To examine the application of the two-dimensional inverse scheme to a three-dimensional problems, we consider an extinction coefficient, $\beta = \beta_1$, which is independent of *z*. Because the medium is finite in the z-direction, this case is still three-dimensional. Hence, we apply both the two-dimensional and three-dimensional inverse scheme to this case, and examine the performance of the two schemes. We first use the three-dimensional forward scheme and make the incidence at three axial positions, $z = 0.5$, 0.75 and 0.95. By collecting the data around the incident planes, we perform the 3-D reconstruction. Then, we use measured data at each incident plane for the two-dimensional

reconstruction of radiation parameters, similar to (Ou and Wu, 2002). Fig. 8(a) show the comparison of the exact β_1 and the reconstructed results obtained by the two-dimensional inverse scheme. The results obtained by using the measured data collected at the center boundary ($z = 0.5$) of the medium are in good agreement with the exact β_1 and more accurate than those obtained by using other data. The results get worse, when the incident position moving far away from the plane $z = 0.5$, as shown in Fig. 8(a). This is because more radiation escapes from the end of a finite-length column although and the two-dimensional scheme became less valid there. However, Fig. 8(b) shows that the two-dimensional reconstructed results are nearly coincide at the center plane ($z = 0.5$), where the three-dimensional effects are weak.

Next, we consider the simultaneously estimation of the spatially variable distributions of extinction coefficient ($\beta = \beta_1$) and albedo ($\omega = \omega_2$) under known phase function ($\Phi = \Phi_f$). We take $\hat{M}_\omega \times \hat{N}_\omega = 5 \times 3$ and $\hat{M}_\beta \times \hat{N}_\beta \times \hat{L}_\beta = 5 \times 3 \times 3$ to reconstruct these distributions. Fig. 9(a) shows that reconstructed distribution of albedo coincides with the exact one. The results shown in Fig. 9(b) show that the reconstructed distribution of extinction coefficient appears similar distribution of discrepancy between the exact and estimated $\beta's$ as in Fig. 7(a) and Fig 8(a).

To investigate the estimation of ω further, we consider the case with the same size and β, but with a less smooth distribution of albedo, $\omega = \omega_3$. Figs. 10(a) and (b) show the estimated albedo along the *x*- and *y*-axis, respectively. Curves of the estimated albedo have little osculation near the points where the exact albedo has a discontinuous first order derivation. Figs. 10(c) and 10(d) show that the estimated $\hat{\beta}$ are in agreement with the exact β. The discrepancies between the exact and estimated values of $\beta's$ are not larger than those found in the case with a smooth albedo (Fig. 9). Therefore, the error caused by the estimated albedo does not result in the increase of error to the estimated extinction coefficient.

The effects of measurement errors on the accuracy of the estimation are also investigated. The simulated measured leaving radiative fluxes with errors ($\tilde{q}^i$) are obtained by adding normal distributed errors to the leaving radiative fluxes (q^i_{exact}) obtained by solving the forward

problem with a high-order ($N_{\psi_x} \times M_\theta = 12 \times 5$) scheme and given exact β , ω and Φ . That is, $\tilde{q}^i = q^i_{\text{exact}}(1+\sigma\,\varsigma)$, (14)

where σ is the standard deviation of the measurement data, and ς is a normal distributed random variable with zero mean and unit standard deviation. Finally, we consider reconstructing the cases with $\beta = \beta_3$, $\omega = \omega_3$ and $\Phi = \Phi_f$ and the values of σ are 0.01 and 0.005, respectively. The reconstructed distributions of extinction coefficient and albedo along x axis on the plane $z = 0.5$ and phase function are shown in Figs. 11(a), 11(b) and 11(c) respectively. The results reveal that (i) the discrepancies between the estimated and exact values of β and ω increase with the increase of the values of σ, (ii) the reconstructed coefficients of the expanded phase functions are less sensitive to the measurement error, (iii) the accuracy of results of these simultaneously estimation cases are acceptable for $\sigma < 0.01$.

IV. CONCLUSIONS

Property reconstruction for a three-dimensional medium with a complete scattering model is investigated by solving the Boltzmann transport equation and an optimization-based reconstruction schemes. The forward problem is solved by a modified discrete-ordinate method (MDOM). The inverse problem is formulated as a least square problem that minimizes the discrepancy between the measured and the calculated leaving radiative fluxes. The Levenberg-Marquardt algorithm is applied to the least square problems for a variety of cases. Owing to the minimization of objection function is an over-constrained problem, we use optical tomography method to acquire enough information for reconstructing the radiative properties. Based on the results obtained, the following conclusions can be drawn.

(i) More discrete directions and more cells of the domain are necessary for accurate computation, when the distributions of radiative properties are more non-uniform.

(ii) For three-dimensional cases, when energy dissipation from both ends and abrupt variation due to finite length in z-direction for radiation intensity are considearable, it is not suitable to reconstruct the distribution of β with a two-dimensional algorithm in place of a three-dimensional algorithm. Otherwise, using the two-dimensional algorithm in place of the three-dimensional algorithm may generate accurate enough results and save computational time.

(iii) When the albedo has a discontinuous first order derivation, curves of the estimated albedo have little osculation, but the error caused by the estimated albedo does not result in the increase of error to the estimated extinction coefficient.

(iv) The discrepancies between the estimated and exact values of β and ω increase with the increase of the measurement errors.

(v) The effects of measurement errors on the accuracy of these simultaneously estimation cases are acceptable for $\sigma < 0.01$.

References

[1] Agarwal, B. M., Mengüc, M. P., (1991), "Forward and inverse analysis of single and multiple scattering of collimated radiation in an axisymmetric system," International Journal of Heat and Mass Transfer, Vol. 34, pp. 633-647.

[2] Alpatov, V. V., Romanovsky, Y. A., (1998), "Methods of optical tomography for remote sensing of the atmosphere and near-earth space," Advances in Space Research, Vol. 21, pp. 1437-1440.

[3] Arridge, S. R., (1999), "Optical tomography in medical imaging," Inverse Problem, Vol. 15, pp. R41-R93.

[4] Hill, B. Y., Hayakawa, C. K., You J. S., and Venugopalan, V., (2001), "Recovery of optical absorption, scattering and anisotropy coefficients using photon migration methods," Proceedings of 35th International Heat Transfer Conference, ASME, pp. 1651-1657.

[5] Hsu, S.-C., Wu, C.-Y., and Ou, N.-R., (1998), "Azimuthally dependent radiative transfer in an nonhomogeneous cylindrical medium," Radiation Physics and Chemistry, Vol.53, pp. 107-113.

[6] Hughey, B.J., Santavicca, D.A., (1982), "A comparison of techniques for reconstructing axisymmetric reacting flow fields from absorption measurements," Combustion Science and Technology, Vol. 29, pp. 167-190.

[7] Jiang, H., (1999), "Optical image reconstruction based on the third-order diffusion equations," Optical Express, Vol. 4, pp. 241-246.

[8] Klose, A. D., Hielscher, A. H., (2002), "Optical tomography using the time-independent equation of radiative transfer-part II: Inverse model," Journal of Quantitative Spectroscopy and Radiative Transfer, Vol. 72 pp. 715-732.

[9] Liou B. T., and Wu, C. Y., (1997), "Ray effects in the discrete ordinate solution for surface radiation exchange," Heat and Mass Transfer, Vol.32, pp. 271-275.

[10]Marquardt, D. W., (1963), "An algorithm for least-squares estimation of nonlinear parameters," Journal of the Society for Industrial and Applied

Mathematics, Vol. 11, pp. 431-441.

[11]Ou, N. R., Wu, C. Y., (2002), "Simultaneous estimation of extinction coefficient distribution, scattering albedo and phase function of a two-dimensional medium," International Journal of Heat and Mass Transfer, Vol. 45, pp. 4663-4674.

[12]Ravichandran, M., Gouldin, F. C., (1986), "Determination of temperature and concentration profiles using (a limited number of) absorption measurements," Combustion Science and Technology, Vol. 45, pp. 47-64.

[13]Ripoll, J., Nieto-Versperians, M., Arridge, S. R., and Dehghani, H., (2000), "Boundary conditions for light propagation in diffusive media with nonscattering regions," Journal of the Optical Society of America A, Vol., 17, pp. 1671- 1682

[14]Torniainen, E. D., Gouldin, F. C. (1998), "Tomographic reconstruction of 2-D absorption coefficient distributions from a limited set of infrared absorption data," Combustion Science and Technology, Vol. 131, pp. 85-105.Yamada, Y., "Light-tissue

[15]interaction and optical imaging in biomedicine," in: C. L. Tien ed., *Annual Review of Heat Transfer*, (Begell House, New York, 1995), Vol. 6, Chap. 1.

[16]Yuen, W. W., Ma, A., Hsu, I. C., and Cunnington, G. R. Jr., (1991), "Determination of optical properties by two-dimensional scattering," International Journal of. Thermophysics, Vol. 6, pp. 182-185.

[17]William, H. P., Saul, A. T., William, T. V., and Brain, P. F., (1992), Numerical Recipes, 2nd ed., (Cambridge University Press, New York), Chap. 15.

Table 1. Properties of the media considered

Extinction coefficients
$\beta_1(r,\psi)=\begin{cases}\frac{1125}{128}(\frac{32}{125}-\frac{6}{5}r_1^2+r_1^3)+\frac{1}{10} \\ \text{for } r_1\le 0.8 \\ \frac{1}{10} \\ \text{for } r_1>0.8\end{cases}$
$\beta_2(r,\psi)=\begin{cases}1050(\frac{1}{250}-\frac{3}{10}r_1^2+r_1^3)+\frac{1}{10} \\ \text{for } r_1\le 0.2 \\ \frac{1}{10} \\ \text{for } r_1>0.2\end{cases}$
$\beta_3(r,\psi,z)=\beta_1(r,\psi)\times(0.5+0.5z^2)$
with $r_1=\sqrt{[r\cos(\psi)-\frac{1}{5}]^2+[r\sin(\psi)]^2}$

Scattering phase functions
$\Phi_f=1.0+1.98398P_1(\cos\theta_0)$ $+1.50823P_2(\cos\theta_0)$ $+0.70075P_3(\cos\theta_0)$ $+0.23489P_4(\cos\theta_0)$ $+0.05133P_5(\cos\theta_0)$ $+0.00760P_6(\cos\theta_0)$ $+0.00048P_7(\cos\theta_0)$
with $\theta_0=\cos^{-1}\mu\mu'+\eta\eta'+\xi\xi'$
Scattering albedoes
$\omega_1=0.5$
$\omega_2=0.5+0.4r[\cos(\psi)+0.2\cos(3\psi)]$
$\omega_3(r,\psi)=\begin{cases}0.4(1-4r_1^2)+\frac{1}{2} \\ \text{for } r_1\le 0.5 \\ \frac{1}{2} \\ \text{for } r_1>0.5\end{cases}$

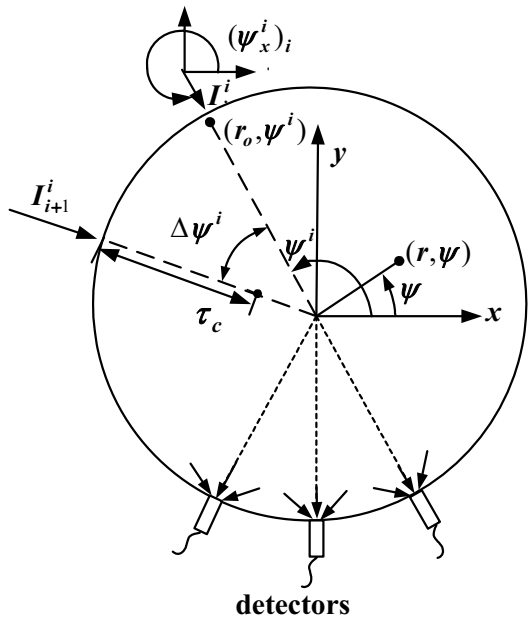

Fig. 1(a) Physical model,

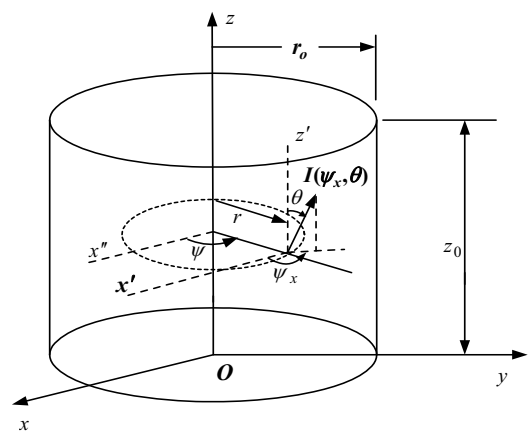

Fig. 1(b) coordinate

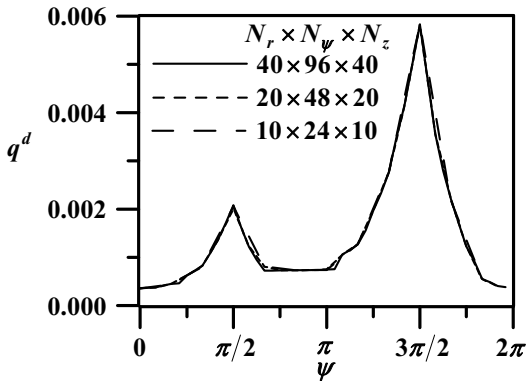

Fig. 2(a) Distributions of the leaving diffuse radiative fluxes with $A=1$, $H=1$, $z_i=0.5$, $\beta=\beta_3$, $\omega=\omega_1$, $\Phi=\Phi_f$, $N_{\psi_x}\times M_\theta=12\times5$ at different sets of cells: at the plane $z=0.5$,

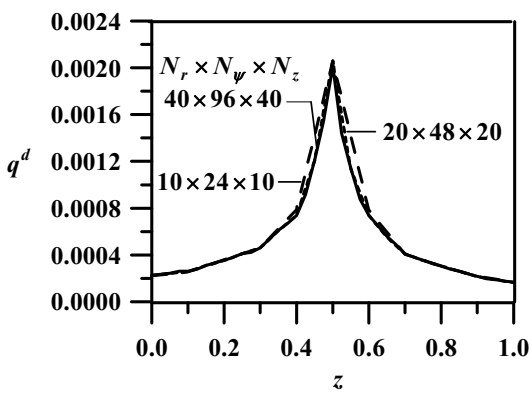

Fig. 2(b) Distributions of the leaving diffuse radiative fluxes with $A=1$, $H=1$, $z_i=0.5$, $\beta=\beta_3$, $\omega=\omega_1$, $\Phi=\Phi_f$, $N_{\psi_x}\times M_\theta=12\times5$ at different sets of cells: along axis $(1,\pi/2,z)$.

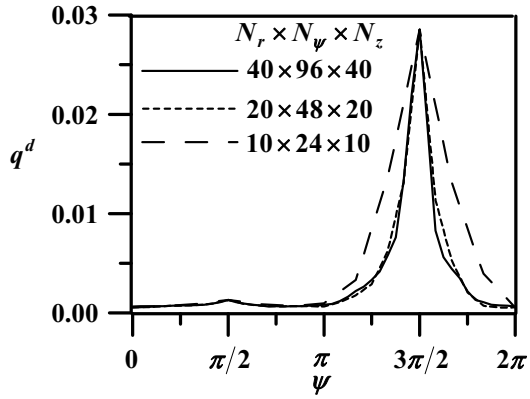

Fig.3(a) Distributions of the leaving diffuse radiative fluxes with $A=1$, $H=1$, $z_i=0.5$, $\beta=\beta_2$, $\omega=\omega_1$, $\Phi=\Phi_f$, $N_{\psi_x}\times M_\theta=12\times5$ at different sets of cells: at the plane $z=0.5$,

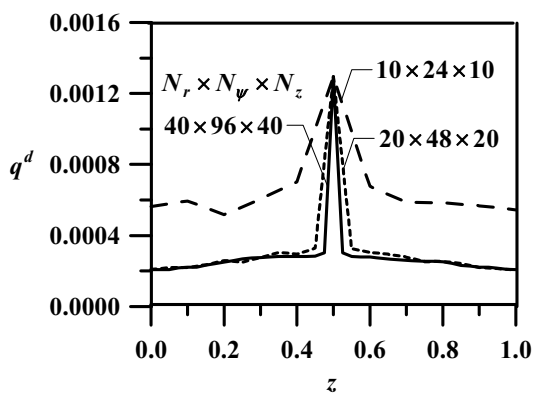

Fig. 3(b) Distributions of the leaving diffuse radiative fluxes with $A=1$, $H=1$, $z_i=0.5$, $\beta=\beta_2$, $\omega=\omega_1$, $\Phi=\Phi_f$, $N_{\psi_x}\times M_\theta=12\times5$ at different sets of cells: along axis $(1,\pi/2,z)$.

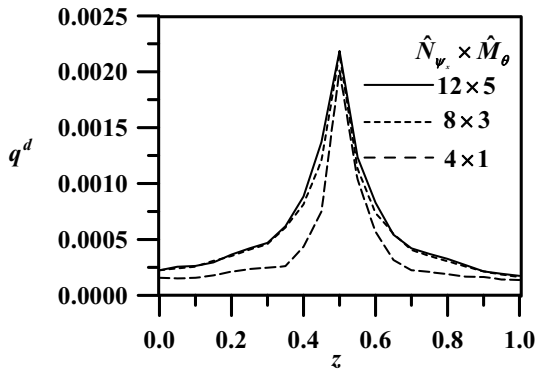

Fig. 4 Distributions of the leaving diffuse radiative fluxes along axis $(1, \pi/2, z)$ with $A = 1$, $H = 1$, $z_i = 0.5$, $\beta = \beta_3$, $\omega = \omega_1$, $\Phi = \Phi_f$, $N_r \times N_\psi \times N_z = 20 \times 48 \times 20$: different sets of discrete ordinate.

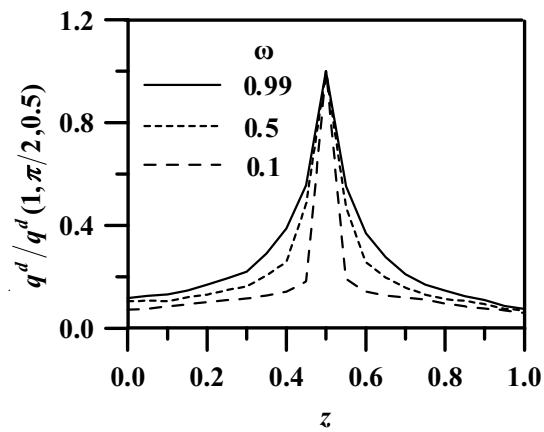

Fig. 5(a) Distributions of the leaving diffuse radiative fluxes ratio for different albedoes with $A = 1$, $H = 1$, $z_i = 0.5$, $\beta = \beta_1$, $\Phi = \Phi_f$, $N_{\psi_x} \times M_\theta = 12 \times 5$, $N_r \times N_\psi \times N_z = 10 \times 24 \times 10$: along axis $(1, \pi/2, z)$,

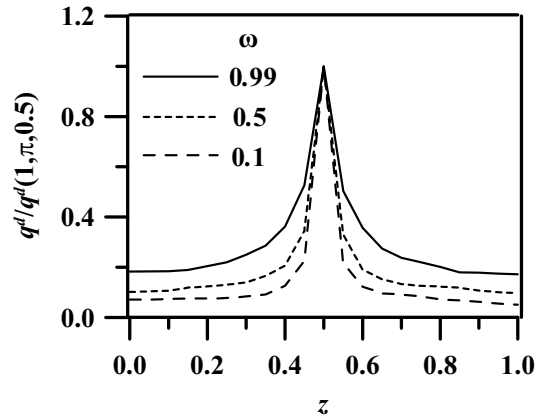

Fig. 5(b) Distributions of the leaving diffuse radiative fluxes ratio for different albedoes with $A = 1$, $H = 1$, $z_i = 0.5$, $\beta = \beta_1$, $\Phi = \Phi_f$, $N_{\psi_x} \times M_\theta = 12 \times 5$, $N_r \times N_\psi \times N_z = 10 \times 24 \times 10$: along axis $(1, \pi, z)$.

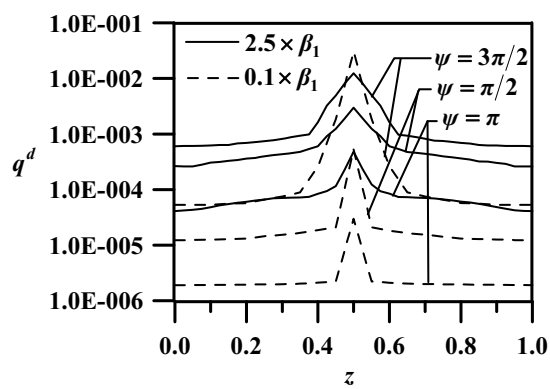

Fig. 6 Distributions of the leaving diffuse radiative fluxes for different optical size with $A = 1$, $H = 1$, $z_i = 0.5$, $\omega = \omega_1$, $\Phi = \Phi_f$, $N_{\psi_x} \times M_\theta = 12 \times 5$: along three different axes -parallel to *z*- axis

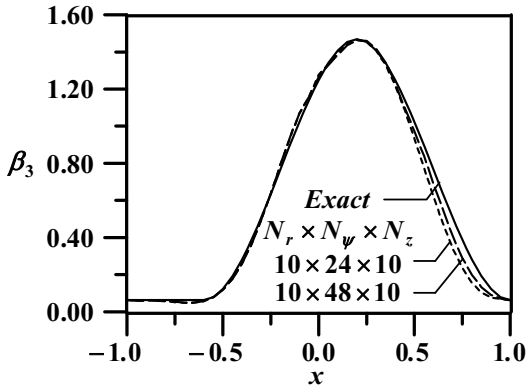

Fig. 7(a) Distributions of the reconstructed β for the case with $\beta = \beta_3$, $\omega = \omega_1$, $\Phi = \Phi_f$, $A = 1$, $H = 1$, $z_i = 0.5$, 0.75, 0.95, $N_{\psi_x} \times M_\theta = 12 \times 5$,: along *x*- axis at the plane $z = 0.5$

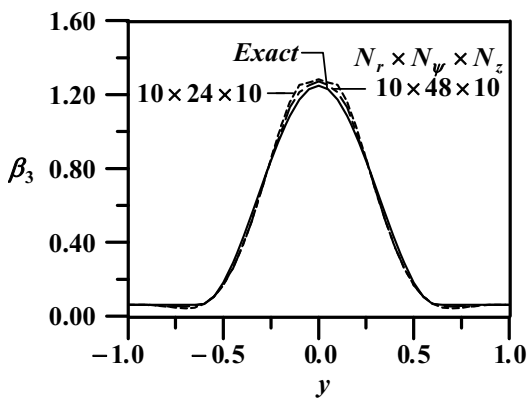

Fig. 7(b) Distributions of the reconstructed β for the case with $\beta = \beta_3$, $\omega = \omega_1$, $\Phi = \Phi_f$, $A = 1$, $H = 1$, $z_i = 0.5$, 0.75, 0.95, $N_{\psi_x} \times M_\theta = 12 \times 5$,: along *y*- axis at the plane $z = 0.5$,

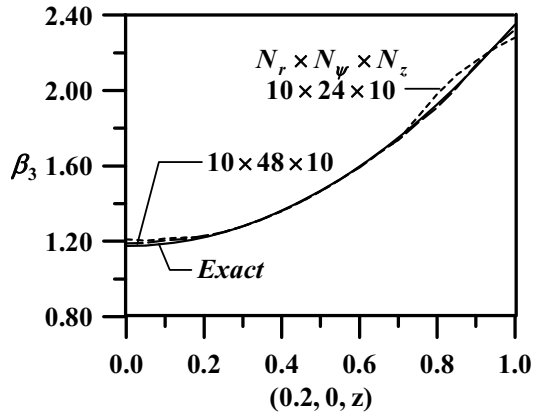

Fig. 7(c) Distributions of the reconstructed β for the case with $\beta = \beta_3$, $\omega = \omega_1$, $\Phi = \Phi_f$, $A = 1$, $H = 1$, $z_i = 0.5$, 0.75, 0.95, $N_{\psi_x} \times M_\theta = 12 \times 5$: along axis $(0.2, 0, z)$.

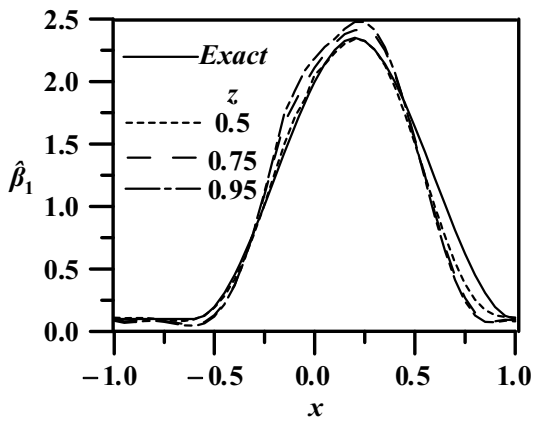

Fig. 8(a) Estimated distributions of β along x axis at different $r - \psi$ plane gained by two dimensional algorithm with $\beta = \beta_1$, $\omega = \omega_1$, $\Phi = \Phi_f$, $A = 1$, $H = 1$, $z_i = 0.5$, 0.75, 0.95, $N_{\psi_x} \times M_\theta = 12 \times 5$, $N_r \times N_\psi \times N_z = 10 \times 24 \times 10$,

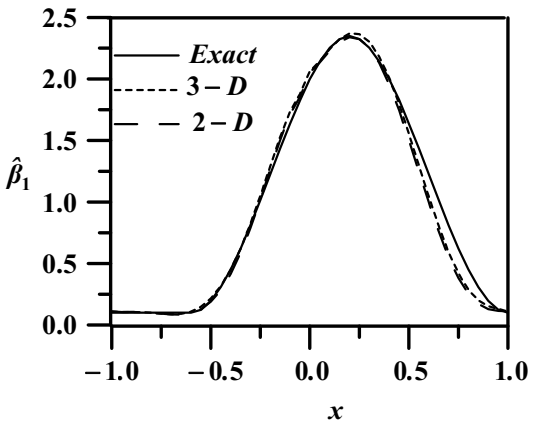

Fig. 8(b) Comparisons of estimated distributions of β along x- axis at $z = 0.5$ plane gained by two- and three-dimensional algorithms with $\beta = \beta_1$, $\omega = \omega_1, \Phi = \Phi_f, A = 1$, $H = 1$, $z_i = 0.5$, 0.75, 0.95, $N_{\psi_x} \times M_\theta = 12 \times 5$.

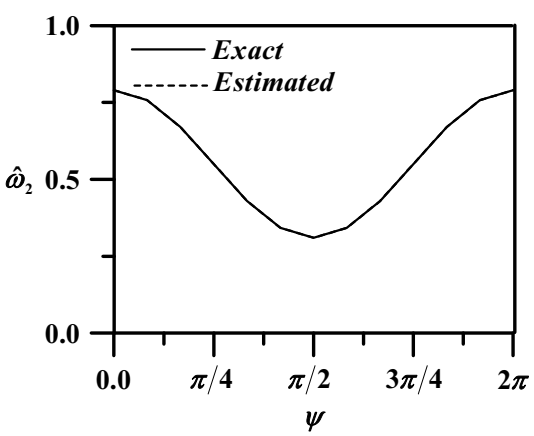

Fig. 9(a) Estimated distributions of ω with $\beta = \beta_1$, $\omega = \omega_2$, $\Phi = \Phi_f$, $A = 1$, $H = 1$, $z_i = 0.5$, 0.75, 0.95: for $r = 0.5$ at the plane $z = 0.5$,

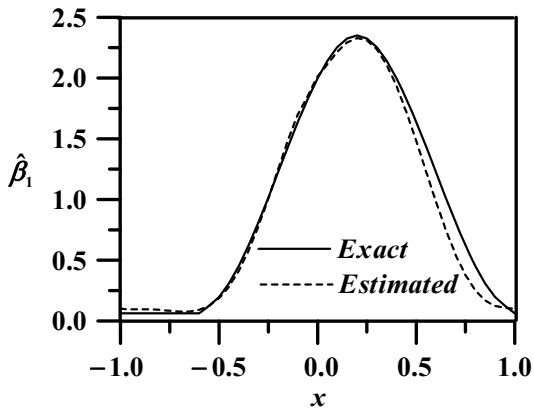

Fig. 9(b) Estimated distributions of β with $\beta = \beta_1$, $\omega = \omega_2$, $\Phi = \Phi_f$ $A = 1$, $H = 1$, $z_i = 0.5$, 0.75, 0.95: along x- axis at the plane $z = 0.5$.

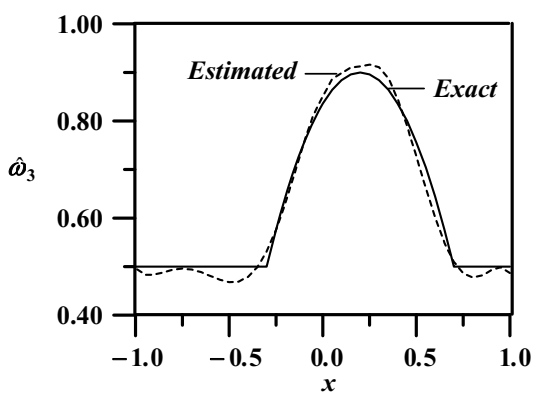

Fig. 10(a) Estimated distributions of ω with $\beta = \beta_1$, $\omega = \omega_3$, $\Phi = \Phi_f$, $A = 1$, $H = 1$, $z_i = 0.5$, 0.75, 0.95: along x-axis at the plane $z = 0.5$,

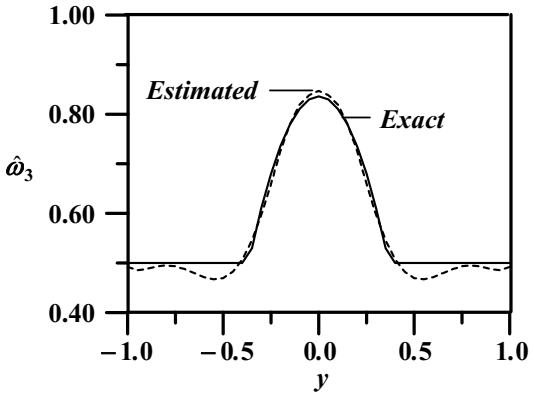

Fig. 10(b) Estimated distributions of ω with $\beta = \beta_1$, $\omega = \omega_3$, $\Phi = \Phi_f$, $A = 1$, $H = 1$, $z_i = 0.5$, 0.75, 0.95: along y-axis at the plane $z = 0.5$,

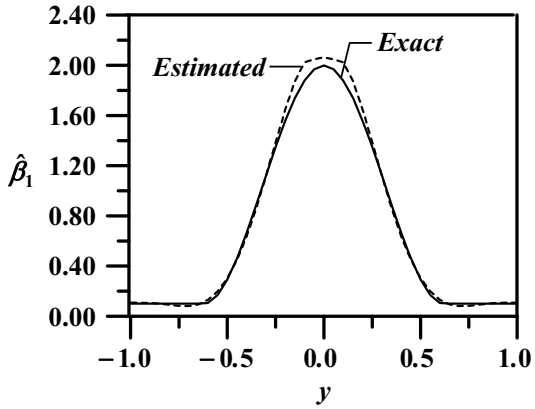

Fig. 10(d) Estimated distributions of β with $\beta = \beta_1$, $\omega = \omega_3$, $\Phi = \Phi_f$, $A = 1$, $H = 1$, $z_i = 0.5$, 0.75, 0.95: along *y*- axis at the plane $z = 0.5$

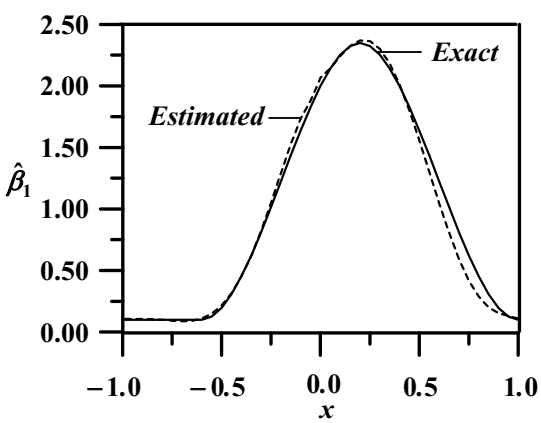

Fig. 10(c) Estimated distributions of β with $\beta = \beta_1$, $\omega = \omega_3$, $\Phi = \Phi_f$, $A = 1$, $H = 1$, $z_i = 0.5$, 0.75, 0.95: along *x*- axis at the plane $z = 0.5$,

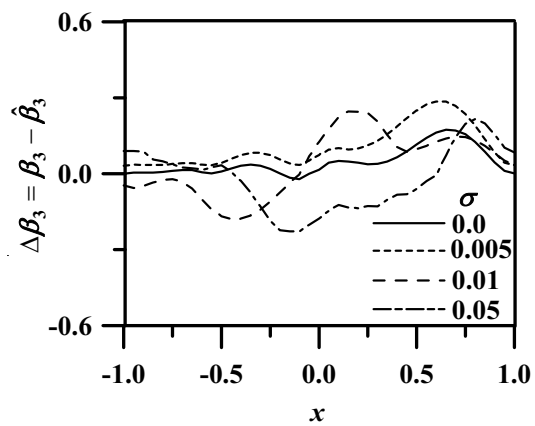

Fig. 11(a) Simultaneously estimation of $\beta = \beta_3$, $\omega = \omega_3$, $\Phi = \Phi_f$ with measurement error for the case with $A = 1$, $H = 1$, $z_i = 0.5$, 0.75, 0.95, $N_{\psi_x} \times M_\theta = 12 \times 5$: distributions of β along *x*- axis at plane $z = 0.5$,

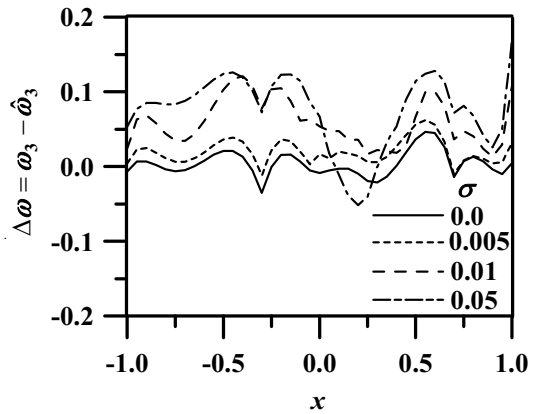

Fig. 11(b) Simultaneously estimation of $\beta = \beta_3$, $\omega = \omega_3$, $\Phi = \Phi_f$ with measurement error for the case with $A = 1$, $H = 1$, $z_i = 0.5$, 0.75, 0.95, $N_{\psi_x} \times M_\theta = 12 \times 5$: differences of exact and estimated distributions of ω along x- axis at plane $z = 0.5$

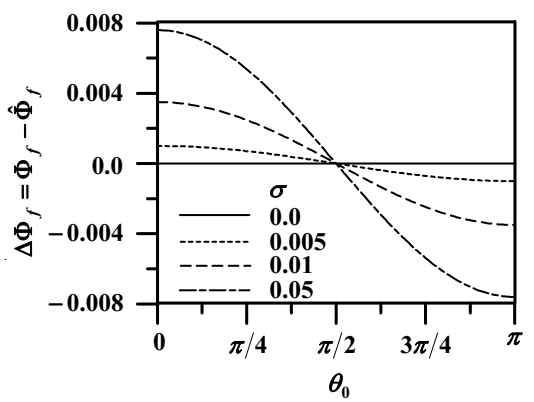

Fig. 11(c) Simultaneously estimation of $\beta = \beta_3$, $\omega = \omega_3$, $\Phi = \Phi_f$ with measurement error for the case with $A = 1$, $H = 1$, $z_i = 0.5$, 0.75, 0.95, $N_{\psi_x} \times M_\theta = 12 \times 5$: differences of exact and estimated distributions of Φ_f